Contribution from the Departments of Chemistry, Washington State University, Pullman, Washington 99164-4630, and Illinois State University, Normal, Illinois 61761

Structure and Magnetism in $ACuCl_3$ Salts Containing Bibridged Chains with Square-Pyramidal Coordination Geometry

U. Geiser,[1a] R. M. Gaura,[1a] R. D. Willett,*[1a] and D. X. West[1b]

Received April 22, 1986

The crystal structure and magnetic behavior of a series of copper chloride salts containing uniform bibridged chains are presented. This includes cyclopentylammonium trichlorocuprate(II), CPAC, and two isomers of *n*-methyl-2-aminopyridinium trichlorocuprate(II) (n = 4, 6), 4MAPC and 6MAPC. CPAC, $(C_5H_{12}N)CuCl_3$, is monoclinic, with space group $P2_1/n$ and lattice parameters a = 10.560 (6) Å, b = 6.089 (1) Å, c = 15.274 (4) Å, β = 106.06 (4)°, V = 943.8 Å^3, and Z = 4. 4MAPC and 6MAPC, $(C_6H_9N_2)CuCl_3$, are isostructural, orthorhombic, with space group *Pnma* and lattice constants a = 11.854 (4)/11.407 (6) Å, b = 6.663 (2)/6.637 (2) Å, c = 12.561 (5)/12.785 (6) Å, V = 992.1/967.9 Å^3, and Z = 4 for the two derivatives, respectively. The magnetic properties of these compounds and of cyclohexylammonium trichlorocuprate(II), CHAC, are deduced from magnetic susceptibility and EPR measurements. Strong exchange coupling exists within the chains (ferromagnetic for CHAC and CPAC, antiferromagnetic for 4MAPC and 6MAPC). It is shown experimentally and theoretically that a correlation exists between the structural characteristics and the magnitude of the exchange coupling. The one-dimensional nature of the systems is confirmed by the analysis of their EPR spectra.

Introduction

The crystal chemistry of copper(II) halides is extremely diverse and varied. Recent interest has been sparked by a variety of phenomena: thermochromism, involving a change in coordination geometry at a phase transition,[2] application of magneto–structural correlations leading to the synthesis of a wide variety of low-dimensional magnetic materials,[3] existence of unusual polymeric species,[4] and relationships to catalytic species of industrial and biological importance,[5,6] to name a few. These phenomena are related to the very flexible stereochemistry of the copper–halide coordination sphere. The copper(II) ion itself has a very flat potential surface, related in part, probably, to the operation of the Jahn–Teller effect and to the relatively small crystal field stabilization of the subsequent distorted coordination geometry. The halide ions themselves, being spherical and monodentate, impose no steric constraints other than those dictated by electrostatic repulsions.

We have recently reviewed the crystal chemistry of $ACuCl_3$ compounds.[7] Two such salts, which have attracted considerable attention because of their magnetic behavior, are cyclohexylammonium trichlorocuprate(II) (henceforth CHAC)[8] and its bromide analogue, CHAB.[9] These chain-type structures have proved to be excellent one-dimensional spin $^1/_2$ Heisenberg ferromagnets. The small XY-like exchange anisotropy in CHAB allowed it to be used by de Jonge and co-workers[9] in a series of experiments that has provided some of the most convincing evidence for the existence of soliton-like excitations in one-dimensional magnetic systems to date. Despite the rather thorough examination of the magnetic properties of CHAC, some confusion still exists concerning the interpretation of the EPR line widths.[10] In this paper we present details of the structures of several of the newer salts mentioned in the recent review,[7] which are closely related structurally to CHAC, namely cyclopentylammonium trichlorocuprate(II) (CPAC), 4-methyl-2-aminopyridinium trichlorocuprate(II) (4MAPC),[11] and 6-methyl-2-aminopyridinium trichlorocuprate(II) (6MAPC).[11] The magnetic properties of these salts are presented along with their EPR spectra. Correlations between the structural and magnetic properties are also given.

Experimental Section

Synthesis. Cyclopentylammonium Trichlorocuprate(II), CPAC. This salt was prepared by mixing stoichiometric amounts of cyclopentylammonium chloride and $CuCl_2 \cdot 2H_2O$ in a mixture of dilute hydrochloric acid and ethanol. Slow evaporation of the solution led to the formation of red, elongated rhombic platelets. They exhibited dichroism (dark red vs. pale red) with maximum absorption parallel to the long crystal direction.

6-Methyl-2-aminopyridinium Trichlorocuprate(II), 6MAPC. 6-Methyl-2-aminopyridinium chloride was prepared by neutralizing the base (Reilly Coal Tar Products, without further purification) in a 1:5 mixture of 12 M hydrochloric acid and propanol. Precipitation of the white hydrochloride was completed by adding acetone. It was filtered, washed with acetone, and dried in air. Equimolar amounts of 6-methyl-2-aminopyridinium chloride and copper(II) chloride were dissolved in propanol and the solutions mixed with stirring at 40 °C. The initially yellow precipitate turned reddish brown after a few minutes. After the mixture was cooled, it was filtered, and the precipitate dried in vacuo overnight. Crystals were grown by dissolving the raw material in slightly acidic (HCl) ethanol at 50 °C and slowly cooling the solution. The crystals of 6-methyl-2-aminopyridinium trichlorocuprate(II) grew as reddish brown elongated platelets. They exhibited noticeable linear dichroism (dark red vs. pale red) under the polarizing microscope. Anal. Found (calcd): C, 25.78 (25.83); H, 3.01 (3.25); N, 10.01 (10.04); Cl, 38.00 (38.11).

4-Methyl-2-aminopyridinium Trichlorocuprate(II), 4MAPC. 4-Methyl-2-aminopyridinium trichlorocuprate(II) was formed under similar conditions. Reddish brown crystals, closely resembling those of the 6-methyl salt, formed upon cooling of an alcohol solution containing 4-methyl-2-aminopyridinium chloride and anhydrous copper(II) chloride in equal proportions. Anal. Found (calcd): C, 25.92 (25.83); H, 3.13 (3.25); N, 10.00 (10.04); Cl, 38.43 (38.11).

X-ray Work. The crystal structures were determined at room temperature (293 ± 2 K). Preliminary results were obtained by Weissenberg and precision film techniques. The data collection was carried out on an automated Picker four-circle diffractometer, controlled by the Oak Ridge program package.[12] The data for CPAC were subsequently recollected on a Nicolet R3m/E system. The orientation matrix and lattice parameters were optimized from the least-squares refinement to the angular settings of 12 (25 for CPAC) carefully centered reflections with high Bragg angles. Details of the data collection are given in Table I. Data collection was carried out with θ–2θ scans and a scan width of 2°. Mo

(1) (a) Washington State University. (b) Illinois State University.
(2) Bloomquist, D. R.; Willett, R. D. *Coord. Chem. Rev.* **1982**, *47*, 125.
(3) Willett, R. D. *NATO ASI ser., Ser. C* **1985**, *No. 140*, 389. Hatfield, W. E. *Ibid.* **1985**, *No. 140*, 555. Willett, R. D.; Landee, C. P. *J. Appl. Phys.* **1981**, *53*, 2004.
(4) See for example: Fletcher, R.; Hansen, J. J.; Livermore, J.; Willett, R. D. *Inorg. Chem.* **1983**, *22*, 330. Geiser, U.; Willett, R. D.; Lindbeck, M.; Emerson, K. *J. Am. Chem. Soc.* **1986**, *108*, 1173.
(5) Davies, G.; El-Sayed, M. A. *Inorg. Chem.* **1983**, *22*, 1257.
(6) Solomon, E. I.; Hare, J. W.; Dooley, D. M.; Dawson, J. H.; Stephens, P. J.; Gray, H. B. *J. Am. Chem. Soc.* **1980**, *102*, 168.
(7) Willett, R. D.; Geiser, U. *Croat. Chem. Acta* **1984**, *57*, 737.
(8) Groenendijk, H. A.; Blöte, H. W. J.; van Duyneveldt, A. J.; Gaura, R. M.; Landee, C. P.; Willett, R. D. *Physica B+C (Amsterdam)* **1981**, *106B+C*, 47.
(9) Kopinga, K.; Tinus, A. M. C.; de Jonge, W. J. M. *Phys. Rev. B: Condens. Matter* **1984**, *29*, 2868.
(10) Poertadji, S.; Ablart, G.; Pescia, J.; Clément, S.; Cheik-Rouhou, A. *J. Phys., Lett.* **1983**, *44*, L561.
(11) Geiser, U.; Willett, R. D. *J. Appl. Phys.* **1984**, *55*, 2407.
(12) Busing, W. R.; Ellison, R. D.; Levy, H. A.; King, S. P.; Roseberry, R. T. Report ORNL-4135; Oak Ridge National Laboratory: Oak Ridge, TN, 1968.

0020-1669/86/1325-4203$01.50/0

Table I. X-ray Data

	4MAPC	6MAPC	CPAC
diffractometer syst	Picker	Picker	Nicolet R3m/E
space group	*Pnma*	*Pnma*	$P2_1/n$
a, Å	11.854 (4)	11.407 (6)	10.560 (6)
b, Å	6.663 (2)	6.637 (2)	6.089 (1)
c, Å	12.561 (5)	12.785 (6)	15.274 (4)
α, deg	90.0	90.0	90.0
β, deg	90.0	90.0	106.06 (4)
γ, deg	90.0	90.0	90.0
V, Å^3	992.1	967.9	943.8
Z	4	4	4
calcd density, g/cm^3	1.87	1.91	1.80
reflecns collected	1695 ($h \geq 0$, $k \geq 0$, $l \geq 0$)	2467 ($h \geq 0$, $k \geq 0$, $l \geq 0$)	1468 ($h \geq 0$, $k \leq 0$)
unique, nonextinct reflecns	1557	2290	1396
reflecns with $F > x\sigma$	1217 ($x = 3$)	1921 ($x = 2$)	1139 ($x = 3$)
μ, cm^{-1}	29.7	30.5	31.5
transmission factors	0.58–0.72	0.35–0.56	0.75–0.84
2θ(max), deg	60	70	45
std reflecns	123, 303, 31$\bar{1}$	240, 511, 026	70$\bar{2}$, 3$\bar{2}$0, 30$\bar{8}$
R	0.054	0.063	0.033
R_w	0.051	0.051	0.038

Kα radiation (λ = 0.71069 Å) was used (Zr filtered on the Picker instrument, graphite monochromator on the Nicolet diffractometer).

The data reduction for the Picker data sets included adjustment to the least-squares linear decay curve obtained from the intensities of 3 standard reflections (measured after every 41 peaks), absorption correction, Lorentz and polarization factors, and cross-scaling of two or three sets with use of different attenuation filters. The standard deviations of the intensities were estimated as $\sigma^2(I) = TC + BC + (0.03I)^2$, where TC is the total count and BC is the background count, $I + TC - BC$. The calculations were carried out on Washington State University's Amdahl V-8 computer under VM-370/CMS using a program package described elsewhere.[13] Scattering factor tables from standard sources for Cu^{2+}, Cl^-, N, C,[14] and H[15] were used. The scattering factors were corrected for anomalous dispersion effects.[14] The agreement factors (R values) are defined as

$$R = \sum(||F_o| - |F_c||)/\sum|F_o| \qquad R_w = (\sum w||F_o| - |F_c||^2/\sum w|F_o|^2)^{1/2}$$

A full-matrix least-squares refinement program minimizing $\sum w||F_o| - |F_c||^2$ with weights of $1/\sigma^2(F_o)$ was used where $\sigma^2(F_o)$ was derived from counting statistics.

For the data set for CPAC, the 3 standard reflections were monitored every 50 reflections, and the SHELXTL[16] package was used for data reduction and refinement. Details of the crystal structure of CHAC were published elsewhere.[8]

Magnetic Measurements. Electron paramagnetic resonance spectra were measured on a Varian E-3 X-band spectrometer. The powdered samples were contained in 4 mm diameter quartz tubes. A small quartz glass Dewar container was used to cool the samples to liquid-nitrogen (77 K) temperatures.

The magnetic susceptibilities were measured on a Princeton Applied Research (PAR) Model 155 vibrating-sample magnetometer. Cryogenic temperatures were achieved in a Janis 153 flow cryostat suitable for work with either helium or nitrogen. A conventional electromagnet capable of applying fields up to 10 kOe (1 T), was utilized and the field calibrated with a Hall probe. The temperature was measured with a germanium resistor. The known susceptibility[17] of freshly prepared $HgCo(SCN)_4$[18] was used for the thermometer calibration. This substance obeys the Curie–Weiss law $\chi_m = 2.351\ (2)\ (T + 1.86\ (1))$ per mole, where χ_m is measured without any diamagnetic corrections. Below 20 K, and at fields of 2000–5000 Oe, the zero-field splitting has to be taken into account.[17] In the liquid-nitrogen range, a thermocouple was also used with the calibration given by the National Bureau of Standards.[19]

(13) Geiser, U.; Willett, R. D.; Gaura, R. M. *Acta Crystallogr., Sect. C: Cryst. Struct. Commun.* **1984**, *C40*, 1346.
(14) *International Tables for X-ray Crystallography*; Kynoch: Birmingham, England, 1962; Vol. III.
(15) Stewart, R. F.; Davidson, E. R.; Simpson, W. T. *J. Chem. Phys.* **1965**, *42*, 3175.
(16) Sheldrick, G. "SHELXTL"; Nicolet Analytical Instruments: Madison, WI, 1984.
(17) Brown, D. B.; Crawford, V. H.; Hall, J. W.; Hatfield, W. E. *J. Phys. Chem.* **1977**, *81*, 1303.
(18) Figgis, B. N.; Nyholm, R. S. *J. Chem. Soc.* **1958**, 4190.
(19) Powell, R. L.; Bunch, M. D.; Corruccini, R. J. *NBS Spec. Publ. (U.S.)* **1968**, *No. 300*, 319–1 (Vol. 2).

Table II. Atomic Coordinates ($\times 10^4$) and Isotropic Thermal Parameters (Å$^2 \times 10^3$) for Cyclopentylammonium Trichlorocuprate(II)

	x	y	z	U^a
Cu	2564 (1)	714 (1)	7667 (1)	33 (1)
Cl(1)	3260 (1)	2615 (2)	9234 (1)	41 (1)
Cl(2)	3790 (1)	3037 (2)	7031 (1)	37 (1)
Cl(3)	832 (1)	3053 (2)	7035 (1)	38 (1)
N	1442 (4)	2654 (8)	4864 (3)	46 (2)
C(1)	2060 (5)	2860 (8)	4100 (4)	48 (2)
C(2)	3470 (6)	3603 (12)	4430 (5)	82 (3)
C(3)	4197 (7)	2459 (15)	3913 (7)	120 (4)
C(4)	3392 (7)	632 (15)	3477 (8)	147 (6)
C(5)	2132 (6)	695 (9)	3632 (4)	63 (2)

[a] Equivalent isotropic U defined as one-third of the trace of the orthogonalized U_{ij} tensor.

Structure Solutions

CPAC. Analysis of the Patterson function generated positional parameters for the Cu and Cl atoms. Several cycles of least-squares refinement of positional and isotropic thermal parameters were performed. The subsequent difference Fourier synthesis yielded the N and C atoms in the framework of the cyclopentylammonium ion. Hydrogen atoms were located upon further refinement and different syntheses. Final refinement of the Nicolet R3m/E data included variation of all positional parameters and anisotropic thermal parameters on the Cu, Cl, N, and C atoms. Protons were refined with rigid-body constraints and isotropic thermal parameters fixed at approximately 1.2 times the corresponding heavy-atom thermal parameter. Final values of $R = 0.033$ and $R_w = 0.038$ were obtained for all reflections with $F \geq 3\sigma$ and $2\theta \leq 45°$. Final positional parameters are presented in Table II, and important interatomic distances and angles are given in Table III.

6MAPC. Copper and chloride coordinates were found from a Patterson synthesis and from direct methods. Carbon and nitrogen atoms were located from subsequent difference Fourier maps. Two scale factors, coordinates, and isotropic, and then anisotropic temperature factors were refined in the centrosymmetric space group *Pnma*, which seemed more appropriate than $Pn2_1a$ from the distribution of the normalized structure factors. Hydrogen atoms were placed at calculated positions before the last refinement cycles and, with the exception of those around the amino nitrogen, refined. The amino group presented some difficulty: The residual electron density is very broad and unstructured. Furthermore, four chlorine atoms are within hydrogen-bonding range. Therefore, disorder of the hydrogen positions was assumed. The indicated positions with fractional occupancy of the out-of-plane hydrogen represent an idealization of the true structure.

The final conventional R value (omitting reflections with $F < 2\sigma(F)$) was 0.063; the weighted R value (R_w) under the same conditions was 0.051. In order to test for the correct space group, the mirror plane was removed and some atoms originally at $y = 0.25$ were displaced to $y = 0.255$. The copper atom remained fixed for origin fixing (polar space group $Pn2_1a$). After convergence was obtained, the atoms were randomly distributed above and below $y = 0.25$ to within 3 standard deviations, and the goodness of fit was not improved. Thus, the centric space group

Table III. Interatomic Distances (Å) and Angles (deg) in Cyclopentylammonium Trichlorocuprate(II)[a]

	Distances		
	Copper Coordination Sphere		
Cu–Cl(1)	2.576 (1)	Cu–Cl(3)	2.308 (1)
Cu–Cl(2)	2.305 (2)	Cu–Cl(3^{i})	2.296 (1)
Cu–Cl(2^{i})	2.298 (1)		
	Intrachain Parameters		
Cu–Cu^{i}	3.084 (1)	Cu–Cl(1)	3.371 (1)
	Cyclopentylammonium Cation		
N–C(1)	1.492 (8)	C(3)–C(4)	1.446 (12)
C(1)–C(2)	1.503 (8)	C(4)–C(5)	1.415 (11)
C(2)–C(3)	1.425 (13)	C(5)–C(1)	1.511 (8)
	Hydrogen-Bonding Contacts		
N–Cl(1)^{iii}	3.233	N–Cl(1)^{v}	3.342
N–Cl(1)^{iv}	3.299		
	Distances Involving Hydrogen Atoms in CPAC		
N–NHA	0.79 (4)	N–NHC	0.94 (5)
N–NHB	0.87 (5)		
	Angles		
	Copper Coordination Sphere		
Cl(1)–Cu–Cl(2)	93.83 (5)	Cl(3)–Cu–Cl(3^{i})	166.82 (3)
Cl(1)–Cu–Cl(2^{i})	99.53 (5)	Cl(2)–Cu–Cl(3^{i})	92.70 (4)
Cl(1)–Cu–Cl(3)	95.78 (5)	Cl(3)–Cu–Cl(2^{i})	93.25 (6)
Cl(1)–Cu–Cl(3^{i})	97.34 (5)	Cl(2)–Cu–Cl(3)	85.27 (6)
Cl(2)–Cu–Cl(2^{i})	166.63 (3)	Cl(2^{i})–Cu–Cl(3′)	85.71 (4)
	Intrachain Parameters		
Cu–Cl(2)–Cu^{i}	84.12 (5)	Cu–Cl(3)–Cu^{i}	84.09 (3)
	Cyclopentylammonium Cation		
N–C(1)–C(2)	111.8 (3)	C(3)–C(4)–C(5)	111.2 (8)
N–C(1)–C(5)	112.7 (5)	C(4)–C(5)–C(1)	106.0 (6)
C(1)–C(2)–C(3)	107.6 (6)	C(5)–C(1)–C(2)	104.2 (5)
C(2)–C(3)–C(4)	107.0 (7)		
	Angles Involving Hydrogen Atoms in CPAC		
Cl(1)–N–NHA	109 (4)	C(1)–N–NHC	113 (4)
C(1)–N–NHB	115 (4)		

[a] Esd's are given in parentheses. Symmetry operations: (i) $-x, -{}^{1}/_{2} + y, {}^{3}/_{2} - z$; (ii) $-x, {}^{1}/_{2} + y, {}^{3}/_{2} - z$; (iii) $-1 + x, {}^{3}/_{2} - y, -{}^{1}/_{2} + z$; (iv) $1 - x, {}^{1}/_{2} + y, {}^{1}/_{2} - z$; (v) $1 - x, -{}^{1}/_{2} + y, {}^{1}/_{2} - z$.

Table IV. Atomic Coordinates ($\times 10^4$) and Isotropic Thermal Parameters (Å^2 $\times$ 10^2) for 6-Methyl-2-aminopyridinium Trichlorocuprate(II)

atom	x/a	y/b	z/c	U^a
Cu	0.47097 (4)	0.25000	0.01832 (4)	0.0191 (1)
Cl(1)	0.30028 (9)	0.25000	0.13702 (9)	0.0343 (3)
Cl(2)	0.58079 (7)	0.50033 (10)	0.09859 (6)	0.0269 (2)
N(1)	0.5577 (3)	0.25000	0.4965 (3)	0.023 (1)
N(2)	0.5134 (4)	0.25000	0.3199 (3)	0.033 (1)
C(1)	0.4770 (4)	0.25000	0.4188 (3)	0.024 (1)
C(2)	0.3580 (4)	0.25000	0.4477 (4)	0.030 (1)
C(3)	0.3298 (4)	0.25000	0.5511 (4)	0.033 (1)
C(4)	0.4159 (4)	0.25000	0.6298 (4)	0.032 (1)
C(5)	0.5315 (4)	0.25000	0.6009 (3)	0.026 (1)
C(6)	0.6304 (5)	0.25000	0.6754 (4)	0.038 (2)

[a] Equivalent isotropic U defined as one-third of the trace of the orthogonalized U_{ij} tensor.

Pnma was confirmed. The final atomic positional and thermal parameters are given in Table IV, whereas relevant bond lengths and angles are given in Table V.

4MAPC. From powder and single-crystal X-ray photographs it was obvious that 4-methyl-2-aminopyridinium trichlorocuprate was similar to the 6-methyl derivative. Copper and chlorine positional parameters were therefore taken from that structure. After initial refinement the counterion was located on a difference Fourier synthesis. Positional and thermal parameters were varied and hydrogen atoms included. From the electron density map no indication for disorder of the methyl group was evident. The amino group, however, showed the same type of disorder as the 6-methyl salt, with four possible arrangements of the hydrogen atoms. The final agreement factors were $R = 0.054$ and $R_w = 0.051$, all reflections with $F < 2\sigma(F)$ being omitted. The largest peaks on the final different map were +0.3 (near N(2)) and −0.2 e/Å^3 (near Cu). Final parameters are given in Table VI and bond lengths and angles in Table VII.

Table V. Interatomic Distances (Å) and Angles (deg) in 6-Methyl-2-aminopyridinium Trichlorocuprate(II)[a]

	Distances		
	Copper Coordination Sphere		
Cu–Cl(1)	2.471 (1)	Cu–Cl(2^{i})	2.311 (1)
Cu–Cl(2)	2.322 (1)		
	Intrachain Parameters		
Cu–Cu^{iii}	3.419 (1)		
	6-Methyl-2-aminopyridinium Cation		
N(1)–C(1)	1.356 (6)	C(3)–C(4)	1.407 (8)
C(1)–N(2)	1.332 (6)	C(4)–C(5)	1.371 (7)
C(1)–C(2)	1.408 (7)	C(5)–N(1)	1.370 (6)
C(2)–C(3)	1.363 (8)	C(5)–C(6)	1.479 (7)
	Angles		
	Copper Coordination Sphere		
Cl(1)–Cu–Cl(2)	98.84 (4)	Cl(i)–Cu–Cl(2^{ii})	91.44 (4)
Cl(1)–Cu–Cl(2^{i})	101.35 (3)	Cl(2)–Cu–Cl(2^{iii})	159.81 (3)
Cl(2)–Cu–Cl(2^{i})	84.90 (3)	Cl(2^{i})–Cu–Cl(2^{iii})	91.71 (4)
	Intrachain Parameters		
Cu^{iii}–Cu–Cu^{iv}	152.51 (3)	Cu–Cl(2)–Cu^{iv}	95.11 (3)
	6-Methyl-2-aminopyridinium Cation		
C(1)–N(1)–C(5)	124.5 (4)	C(2)–C(3)–C(4)	122.0 (4)
C(2)–C(1)–N(1)	117.6 (4)	C(3)–C(4)–C(5)	118.7 (4)
N(2)–C(1)–N(1)	119.0 (4)	C(4)–C(5)–N(1)	118.3 (4)
N(2)–C(1)–C(2)	123.4 (4)	C(4)–C(5)–C(6)	124.2 (5)
C(1)–C(2)–C(3)	118.9 (4)	N(1)–C(5)–C(6)	117.5 (4)

[a] Esd's are given in parentheses. Symmetry operations: (i) $1 - x, 1 - y, -z$; (ii) $x, {}^{1}/_{2} - y, z$; (iii) $1 - x, -{}^{1}/_{2} + y, -z$; (iv) $1 - x, {}^{1}/_{2} + y, -z$; (v) $ {}^{1}/_{2} + x, {}^{1}/_{2} - y, {}^{1}/_{2} - z$.

Table VI. Atomic Coordinates ($\times 10^4$) and Isotropic Thermal Parameters (Å^2 $\times$ 10^2) for 6-Methyl-2-aminopyridinium Trichlorocuprate(II)

atom	x/a	y/b	z/c	U^a
Cu	0.48111 (5)	0.25000	0.02168 (5)	0.0266 (2)
Cl(1)	0.34682 (10)	0.25000	0.17186 (10)	0.0426 (4)
Cl(2)	0.60206 (8)	0.50023 (13)	0.08069 (7)	0.0374 (3)
N(1)	0.6389 (4)	0.25000	0.4963 (3)	0.036 (1)
N(2)	0.5685 (4)	0.25000	0.3252 (4)	0.038 (1)
C(1)	0.5486 (4)	0.25000	0.4289 (4)	0.030 (1)
C(2)	0.4405 (4)	0.25000	0.4752 (5)	0.036 (1)
C(3)	0.4263 (4)	0.25000	0.5846 (4)	0.033 (1)
C(4)	0.5240 (5)	0.25000	0.6481 (5)	0.044 (1)
C(5)	0.6272 (5)	0.25000	0.6042 (5)	0.044 (2)
C(6)	0.3122 (5)	0.25000	0.6337 (6)	0.050 (2)

[a] Equivalent isotropic U defined as one-third of the trace of the orthogonalized U_{ij} tensor.

Structure Descriptions

The structures of all four salts, CHAC, CPAC, 4MAPC, and 6MAPC, contain well-isolated, bibridged linear chains of stoichiometry $(CuCl_3)_n^{n-}$. Each copper ion has a square-pyramidal coordination geometry (Figure 1b,c and Table VIII), with the axial bond substantially longer than the basal bonds. The direction of the axial bond alternates along the chain in all four compounds. The structures differ principally in two ways: the nature of the Cu_2Cl_2 bridging unit and the packing arrangement of the chains. Descriptions of the latter will be given in the subsequent section, which gives details of each structure.

In the *n*MAPC salts, the Cu_2Cl_2 bridging unit is planar, while in CHAC and CPAC, this unit is folded across the Cl–Cl line. This is defined by the dihedral angle, δ, between the two $CuCl_2$ planes in the bridge, which are given in Table VIII. The folding leads to a shortening of the intrachain Cu–Cu distance as compared to a stretched structure. Since the interior Cl–Cu–Cl angles are nearly the same in all four salts, this is associated with a

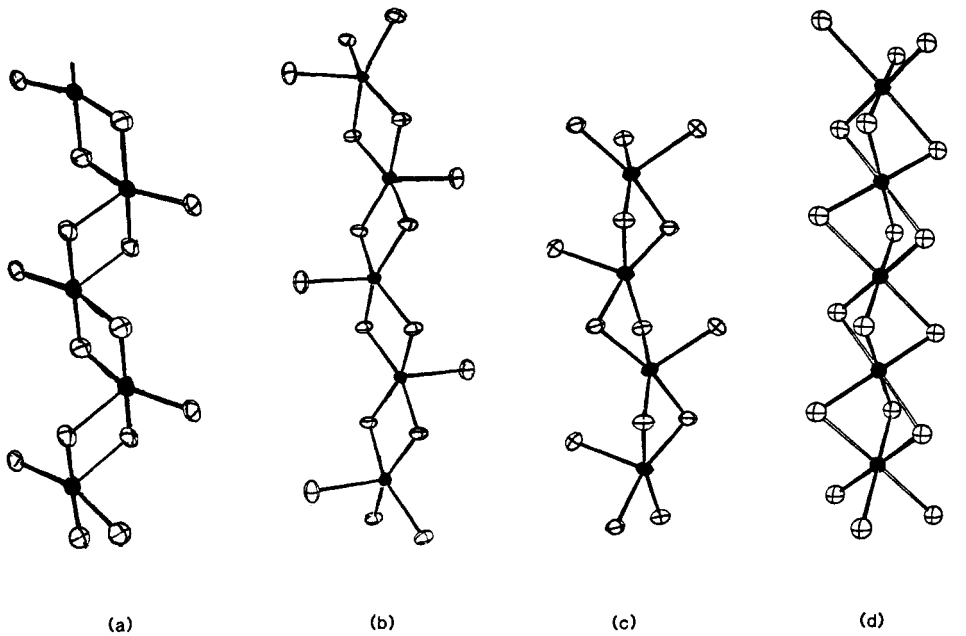

Figure 1. Comparison of the structures of $(CuCl_3)_n^{n-}$ chains: (a) the alternating chain (bibridged chain of dimers) in the low-temperature form of $(CH_3)_2CHNH_3CuCl_3$; (b) uniform chain in 6MAPC; (c) uniform chain in CHAC; (d) tribridged chain in the high-temperature form of $(CH_3)_2CHNH_3CuCl_3$.

Table VII. Interatomic Distances (Å) and Angles (deg) in 4-Methyl-2-aminopyridinium Trichlorocuprate(II)[a]

	Distances		
	Copper Coordination Sphere		
Cu–Cl(1)	2.468 (2)	Cu–Cl(2^{i})	2.323 (1)
Cu–Cl(2)	2.320 (1)		
	Intrachain Parameters		
Cu–Cu^{iii}	3.405 (1)		
	4-Methyl-2-aminopyridinium Cation		
N(1)–C(1)	1.365 (7)	C(3)–C(4)	1.406 (8)
C(1)–N(2)	1.323 (7)	C(4)–C(5)	1.342 (8)
C(1)–C(2)	1.407 (7)	C(5)–N(1)	1.362 (7)
C(2)–C(3)	1.385 (8)	C(3)–C(6)	1.486 (8)
	Angles		
	Copper Coordination Sphere		
Cl(1)–Cu–Cl(2)	98.87 (4)	Cl(2)–Cu–Cl(2^{ii})	91.86 (5)
Cl(1)–Cu–Cl(2^{i})	98.59 (4)	Cl(2)–Cu–Cl(2^{iii})	162.53 (3)
Cl(2)–Cu–Cl(2^{i})	85.65 (4)	Cl(2^{i})–Cu–Cl(2^{iii})	91.53 (5)
	Intrachain Parameters		
Cu^{iii}–Cu–Cu^{iv}	156.10 (4)	Cu–Cl(2)–Cu^{iv}	94.35 (4)
	4-Methyl-2-aminopyridinium Cation		
C(1)–N(1)–C(5)	122.5 (5)	C(2)–C(3)–C(4)	117.6 (4)
C(2)–C(1)–N(1)	117.2 (5)	C(3)–C(4)–C(5)	121.2 (6)
N(2)–C(1)–N(1)	118.1 (5)	C(4)–C(5)–N(1)	120.1 (5)
N(2)–C(1)–C(2)	124.7 (5)	C(2)–C(3)–C(6)	121.5 (5)
C(1)–C(2)–C(3)	121.4 (5)	C(4)–C(3)–C(6)	120.9 (6)

[a] Esd's are given in parentheses. Symmetry operations: (i) $1-x, 1-y, -z$; (ii) $x, {}^1/_2-y, z$; (iii) $1-x, -{}^1/_2+y, -z$; (iv) $1-x, {}^1/_2+y, -z$; (v) ${}^1/_2+x, {}^1/_2-y, {}^1/_2-z$.

decrease in the bridging Cu–Cl–Cu angles as the entity is folded. Furthermore, the folding causes the axial chloride ion to encroach upon the coordination sphere of a neighboring copper ion. A number of trends related to the copper(II) ion stereochemistry are also evident from the examination of Table VIII. The Cu–Cl_{axial} distances are longer in the chains with the folded bridges, and the Cu–Cl_{eq} distances generally shorten as the Cu–Cl_{axial} distances become longer. Also, as the Cu–Cl_{axial} distances become longer, the Cu atoms become closer to the basal plane.

CPAC. The square-pyramidal coordination geometry assumed by the Cu(II) ion in CPAC is virtually identical with that in CHAC,[8] with a slight lengthening of the Cu–Cl_{ax} (0.012 Å) distances occurring in CPAC. The Cu(II) ion sits 0.266 Å above the plane of the equatorial chloride ions in CPAC, and the Cl_{ax}–Cu–Cl_{eq} bond angles average 96.62°. The corresponding values in CHAC are 0.276 Å and 96.87°. The bibridged arrangement of the chain (Figure 1) imposes a C_{2v} distortion upon the basic square-pyramidal geometry, with the interior Cl_{eq}–Cu–Cl_{eq} angles averaging 84.08° in CPAC. The dihedral angle, δ, as described above, is 131.6°. These distortions are significantly larger in CPAC than in CHAC (85.62 and 135.2°, respectively) and lead to a significantly shorter Cu···Cl_{ax} distance between adjacent coordination spheres (3.370 Å in CPAC vs. 3.477 Å in CHAC) and shorter Cu···Cu distances (3.083 vs. 3.138 Å). In all, the chain in CPAC is compressed axially toward a tribridged chain and the coordination sphere in CPAC is significantly closer to square bipyramidal than that in CHAC.

Table VIII. Comparison of Structural and Magnetic Parameters

	CPAC	CHAC	4MAPC	6MAPC
Cu–Cl_{eq} (av), Å	2.302	2.310	2.322	2.316
Cu–Cl_{ax}, Å	2.576	2.564	2.468	2.471
Cl_{eq}–Cu–Cl_{eq} (interior), deg	85.49	85.38	85.65	84.90
Cl_{ax}–Cu–Cu_{eq} (av), deg	96.62	96.87	98.73	100.10
Cu–basal plane, Å	0.258	0.276	0.353	0.406
Cu–Cu, Å	3.084	3.138	3.405	3.419
Cu–Cl–Cu (av), deg	84.10	85.62	94.35	95.11
δ, deg	131.6	135.2	180.0	180.0
J/k, K	~+45	+45	−48	−55
T_c, K	2.78	2.17		
H_c, Oe	200	961		
$z_F J_F$, K		0.15		
$z_{AF}J_{AF}$, K	2.9×10^{-2}	-1.4×10^{-2}	<0.05	<0.05
$\Delta\epsilon$, meV	−0.0318	0.0143	0.0767	0.0852

The chain packing is dictated by the steric and hydrogen bonding constraints imposed by the cyclopentylammonium ions. Along the *c* direction, adjacent chains are hydrogen-bonded together via the $-NH_3$ moieties of the cyclopentylammonium ion. Each of the three hydrogen atoms participates in a hydrogen bond to an axial chloride ion, Cl(1), one bond to one chain and two bonds to an adjacent chain. These adjacent chains are related by centers of inversion. Sheets of chains thus produced are separated by interwoven cyclopentyl groups (Figure 2) forming a layer structure in which adjacent sheets are separated by a unit cell translation in the *a* direction. This packing and hydrogen-

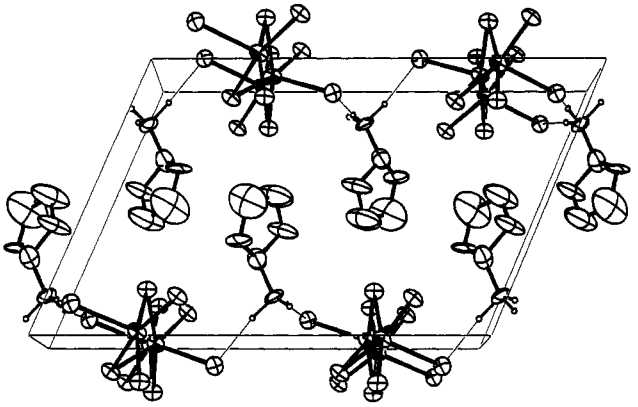

Figure 2. View of the unit cell of cyclopentylammonium trichlorocuprate(II), as seen from the *b* direction. The *c* axis is horizontal.

bonding structure is clearly reflected in the crystal habit since crystals tend to grow as thin platelets, parallel to the *bc* plane and elongated in the chain (*b*) direction. Qualitatively, this packing is similar to that in CHAC. However, the space group for CHAC ($P2_12_12_1$) requires adjacent chains in the sheets to be related by 2_1 screw axes (and not inversion centers as in CPAC) as are adjacent sheets (and not unit cell translations).

It is of interest to note that all of the hydrogen bonds are directed toward the axial chloride ions. In contrast, the equatorial chloride ions form bridges to adjacent copper ions. Thus, the bridging produces a balance of the electrostatic forces in that region of space. The hydrogen bonding is necessary to provide electroneutrality for the axial chloride ion and stabilize the structure.

Both the carbon thermal ellipsoids (Figure 2) and the C–C bond distances and angles (Table III) are indicative of disorder in the cyclopentyl ring. From the crystallographic data, it appears that the C(2)–C(3)–C(4)–C(5) portion of the ring is nearly planar but with very large thermal displacements from that plane. From other crystal structure determinations, it is known that the C(3)–C(4) segment must be twisted out of this plane. Since this twist motion is fourfold degenerate, it is clear that the crystallographic results are measuring an average of the four conformations. This leads to the apparent shortening of the C–C bonds in this segment of the ring.

6MAPC. The most important finding of this structure determination is the geometry of the chain of bibridged square-pyramidal copper chloride complexes (see Figure 1). In contrast to the case for CHAC and CPAC, the bridging geometry here is centrosymmetric, and the bridging angle is well above 90°. The only symmetry element passing through the copper atoms is a mirror plane. However, the point symmetry is nearly C_{2v}, as illustrated by the very similar Cu–Cl(2) distances and Cl(2)–Cu–Cl(2) angles. The Cu–Cl(1) direction forms an angle of 1.8° with the normal to the base plane through the four Cl(2) atoms, and it is tilted toward the farther Cl(2) atoms. The copper atom lies 0.406 (1) Å above the mentioned plane. As seen in Figure 3, the Cu–Cl(1) directions on adjacent chains are nearly perpendicular to each other.

The organic cation is located on the mirror plane, except for some hydrogen atoms. The interatomic distances and angles are in their usual range considering the asymmetric substitution of the pyridine ring. Subsequent cations are stacked on top of each other along the *b* direction, related by a twofold screw axis. The distance between them is half a unit cell translation, or 3.32 Å. The atoms associated with one mirror plane through the crystal are shown in Figure 3. As indicated above, the amino hydrogen coordinates were not refined because of the apparent, but unresolved, disorder. From the various nitrogen–chlorine contacts the presence of hydrogen bonding is mandatory. The projection along C(1)–N(2) shows four chlorine atoms within 3.4 Å. The in-plane Cl(1) atoms are in a more favorable position because of the angles C(1)–N(2)–Cl(1), which are both within 11° of 109.5° (ideal tetrahedral arrangement). The corresponding angle to the out-of-plane chlorine atoms is 150° and hydrogen bonding less likely. However, because of the stereochemistry of the $-NH_2$ group, both its hydrogen atoms cannot be positioned on the mirror plane (i.e. directed toward apical chloride ions) simultaneously, and the assumption of disorder is justified. There is no problem with N(1), where a chlorine atom Cl(1) is 3.24 Å almost exactly along the calculated N–H direction. Again, all hydrogen bonding is directed toward the apical chloride ion, to satisfy electrostatic requirements.

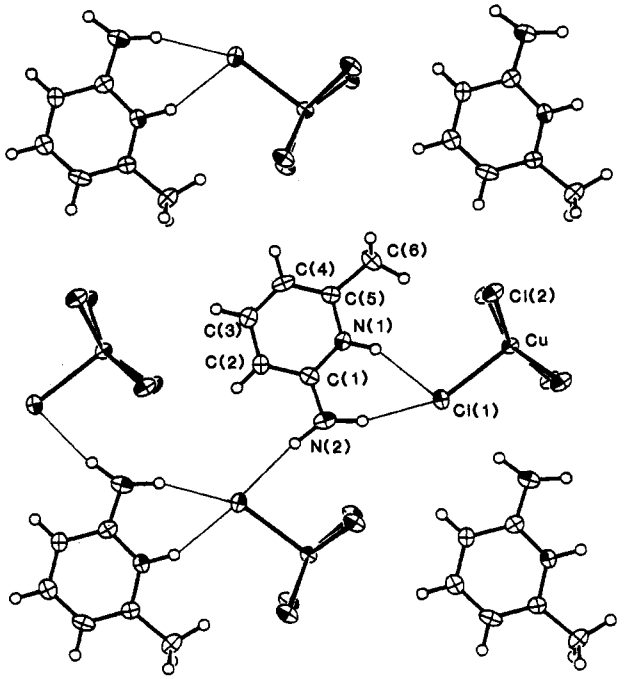

Figure 3. View of the *ac* plane of 6-methyl-2-aminopyridinium trichlorocuprate(II). The *a* axis is horizontal.

Whatever the details of hydrogen bonding may be, it is ultimately responsible for the interactions between the copper chloride chains. The hydrogen-bonding network primarily connects adjacent chains along the diagonals in the *ac* plane. Unlike the case for CHAC and CPAC, there is no direction where there is only electrostatic through-space or van der Waals interaction.

4MAPC. As expected, this structure bears great resemblance to that of the 6-methyl salt, described in the previous section. Corresponding bond lengths are virtually indistinguishable between the two compounds, but a slight variation in angles is evident: The quadrangle formed by two adjacent copper atoms and the bridging chlorine atoms is more quadratic in the 4MAPC compound than in the 6-methyl derivative. The local geometry around the copper atom is even more nearly C_{2v} in 4MAPC, as reflected in the close resemblance of Cl(2)–Cu–Cl(2^{ii}) with Cl(2^{i})–Cu–Cl(2^{iii}) and Cl(1)–Cu–Cl(2) with Cl(1)–Cu–Cl(2^{i}). These angles are within 0.3° of each other, whereas the differences in the 6-methyl compound are up to 2.5°. The point is further exemplified by the fact that the Cu–Cl(1) vector forms an angle of no more than 0.5° with the normal to the basal plane of the pyramid, as compared to 1.8° found in the other salt. The distance of the copper atom from the base plane is 0.353 (1) Å, and the Cu–Cl(1) direction forms an angle of 49.84° with the *a* axis. Discussion of the cation and its hydrogen bonding (Figure 4) follow that for 6MAPC.

Interrelationships in Chain Structures. It is of interest to compare the two chains described here with two other types. These are the alternating chain (a chain of $Cu_2Cl_6^{2-}$ dimers) as in the low-temperature form of $[(CH_3)_2CHNH_3]CuCl_3$[20] in Figure 1a, the *n*MAPC type chains in Figure 1b, the CHAC, CPAC type chains in Figure 1c, and a tribridged chain as in the high-temperature form of $[(CH_3)_2CHNH_3]CuCl_3$[21] in Figure 1d. If one

(20) Willett, R. D. *J. Chem. Phys.* **1966**, *45*, 3737.
(21) Roberts, S. A.; Bloomquist, D. R.; Willett, R. D.; Dodgen, H. W. *J. Am. Chem. Soc.* **1981**, *103*, 2603.

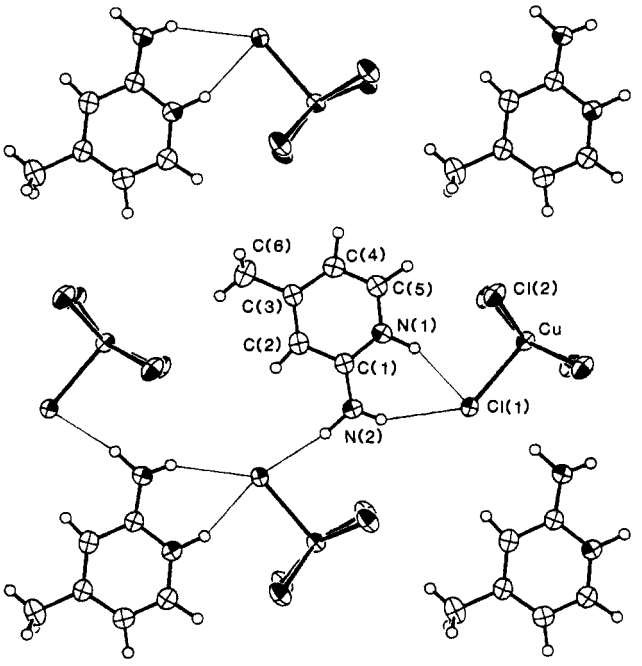

Figure 4. View of the *ac* plane of 4-methyl-2-aminopyridinium trichlorocuprate(II). The *a* axis is horizontal.

starts with the *n*MAPC chain with square-pyramidal coordination, it can be envisioned that a compression of the chain will lead to the accordion-type folding of the chain as observed in CHAC and CPAC. In this latter type, the axial chloride approaches a neighboring copper ion, but at a distance long enough that no significant distortion of the square-pyramidal coordination, e.g., the reduction of the Cl_{ax}–Cu–Cl_{eq} angles toward 90°, occurs. Furthermore, the distance between the coordinated and the approaching chlorine atoms exceeds the sum of the van der Waals radii. A further folding of the chain would yield a six-coordinate species for each copper center that upon the reorientation of the Jahn–Teller elongation axes, can yield the tribridged structure in Figure 1d. On the other hand, starting with the *n*MAPC chains, an interchange of the axial bond with one of the equatorial bonds at each copper site yields the dimer chain in Figure 1a. Finally, it is noted that, in $(CH_3)_2CHNH_3CuCl_3$, the dimer chain undergoes a phase transition directly to the tribridged chain.[21]

As pointed out in ref 2 and 7, the stabilization of the bibridged structures can be rationalized in terms of charge compensation arguments—in this case, the ability of the organic cations to hydrogen bond to the nonbridging halide ions. If a halide is involved in several strong hydrogen bonds, as is the case for the axial chloride ions in all the compounds described here, its negative charge is partially neutralized, and it is not energetically favorable for it to form a bridge to an adjacent copper ion.

Magnetic Results

Before we begin the discussion of the magnetic properties of CPAC, a brief summary of the behavior of CHAC[8] is in order. The $(CuCl_3)_n^{n-}$ chains run parallel to the *c* axis in CHAC (orthorhombic crystal system, space group $P2_12_12_1$) with strong ($J/k \approx 50$ K) intrachain coupling based on an empirical Hamiltonian $\mathcal{H}_{ex} = -2J\bar{S}_i\bar{S}_j$. Adjacent chains in the *bc* plane are hydrogen bonded together, with an interchain coupling $J' = J_F = 0.15$ K. CHA ions interleave between planes in the *a* direction, leading to a weak antiferromagnetic coupling of dipolar origin ($z_{AF}J_{AF} = -1.44 \times 10^{-2}$ K) between chains. Since adjacent chains in the *a* direction are related by a 2_1 screw axis, spin canting is allowed, and a weak ferromagnetic moment parallel to the *a* axis is observed. These structural characteristics lead to metamagnetic behavior with a critical field (parallel to the *b* axis) of 96 Oe and 3d antiferromagnetic ordering at $T_N = 2.17$ K. In CPAC, the chain and hydrogen-bonding structure are nearly identical (with the *b* and *c* axes switched in orientation). However, adjacent

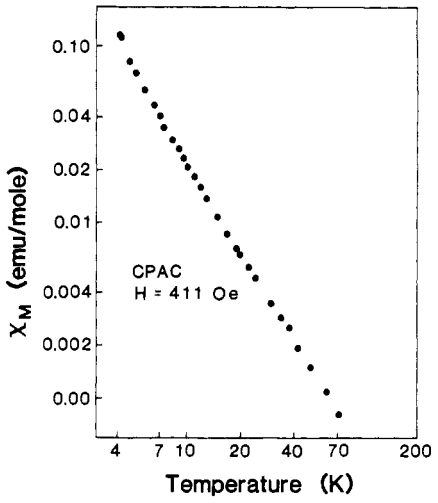

Figure 5. log–log plot of χ_m vs. T for CPAC.

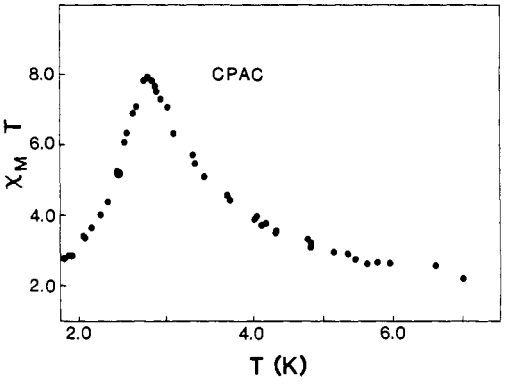

Figure 6. Plot of $\chi_m T$ vs. T for CPAC in the low-temperature region.

chains in the *a* direction are related by centers of inversion, so that the dipolar interactions must lead to a collinear spin arrangement. Thus, CPAC is not expected to show overt spin canting but can exhibit metamagnetic behavior.

CPAC. In order to magnetically characterize CPAC, we need to determine signs and magnitudes of three exchange constants: J, the intrachain interaction; J_c, the interchain interaction within the sheets; and J_a, the interchain interaction between sheets. The sign of J is readily found to be positive (ferromagnetic) from the magnetic susceptibility data since the product χT increases rapidly as the temperature is lowered. The data in the 4.2–100 K range exhibit a $T^{-1.7}$ dependence (Figure 5), in good agreement with theoretical predictions for a one-dimensional system with ferromagnetic coupling.[24] In that region, χ for CPAC is virtually superimposable upon the data for the corresponding CHAC and CHAB salts. For the latter, $J/k = 45 \pm 5$ and 55 ± 5 K, respectively, from heat capacity measurements.[9,22] At intermediate temperatures, the powder susceptibility of CPAC is about 2% larger than that of CHAC, indicating that $J/k \approx 45$–50 K. A detailed fit was not attempted since the correlation between J and g (and other factors that affect the magnitude of the high-temperature susceptibility) is extremely high, making values obtained from fitting the susceptibility extremely unreliable (for example, changing the value of the TIP correction to CHAC from 60×10^{-6} to 120×10^{-6} emu/mol changed the value of J/k from 55 to 70 K).

Below 4.2 K, the powder susceptibility continues to increase until it reaches a sharp maximum at 2.8 K ($\chi_M T = 8.0$ at the maximum; Figure 6), implying the existence of at least one antiferromagnetic interaction. Thus, CPAC is not quite as good a 1D system as CHAC ($T_N = 2.17$ K). Below 2.8 K, the salt shows

(22) Kopinga, K.; Tinus, A. M. C.; de Jonge, W. J. M. *Phys. Rev. B: Condens. Matter* **1982**, *B25*, 4685.

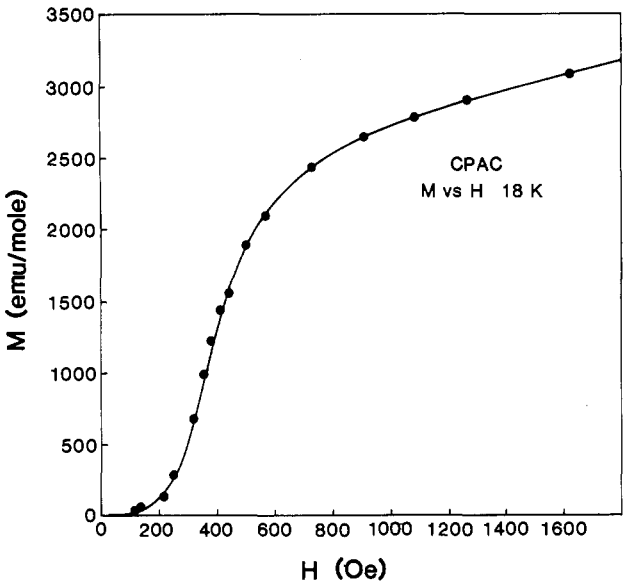

Figure 7. Plot of powder magnetization vs. field for CPAC at 1.8 K. The solid line is a guide to the eye only.

metamagnetic behavior, as seen from the plot of M vs. H in Figure 7 for the powder at 1.8 K. Thus, one of the interchain interactions, J_a or J_c, must be ferromagnetic. The magnetization shows a slow increase from zero up to 200 Oe and then rises rapidly. This corresponds to H_{c1}, the critical field for the transition from the antiferromagnetic ground state to the mixed-phase region. The upper boundary of the mixed-phase region, H_{c2}, is difficult to estimate from the powder data but probably occurs at ~600 Oe. From the mean field relationship for a metamagnet

$$-2z_{AF}J_{AF}S^2/k = g\mu_B SH_{c2}$$

we estimate $z_{AF}J_{AF}/k = -3 \times 10^{-2}$ K. This value is twice as large as in CHAC, not a surprising result since the CPA ion is smaller than the CHA ion, so that the dipolar interactions are expected to be larger. This is also consistent with the increased value of T_c. The fact that $M \rightarrow 0$ as $H \rightarrow 0$ implies the absence of any canting, in agreement with the structural features. In the absence of a detailed phase diagram, e.g., from single-crystal magnetization data, it is impossible to obtain the other interchain exchange constant, J_F. However, it seems reasonable to assume it is of the same order of magnitude as in CHAC, since the hydrogen-bonded exchange pathway is identical. Thus, it is concluded for CPAC that $J/k \approx 500$ K and, by analogy with CHAC, $J_c/k \equiv J_F/k > 0$ (probably ~0.5 K) and $z_aJ_a/k \equiv z_{AF}J_{AF}/k = -3 \times 10^{-2}$ K.

4MAPC and 6MAPC. The magnetic powder susceptibility (Figure 8) of 6-methyl-2-aminopyridinium trichlorocuprate(II) is characterized by low values at high temperatures, a broad maximum around 70 K, and a $1/T$-like divergence as $T \rightarrow 0$. The magnitude of this last value varies from sample to sample. From the crystal structure it is implied that a one-dimensional model is appropriate for this compound. The reduced magnetic moment, as compared to Curie-law behavior, and the broad maximum in the susceptibility suggest a strong antiferromagnetic coupling ($J/k \simeq -55$ K from the location of the maximum). The divergent behavior at low temperature can be rationalized by the presence of a paramagnetic impurity. The nature of this impurity is hard to determine, and it is likely intrinsic in nature, due to interruptions in the chain by crystal imperfections. Fragments with an odd number of copper ions between packing faults will possess a doublet ground state with limiting Curie law at low temperatures. A more accurate value for the exchange parameter J was obtained from the least-squares fitting of the data for the sample with the smallest amount of impurity to the formula

$$\chi = (1 - \alpha)\chi_0 + \alpha Ng^2\mu^2/(4kT)$$

where χ_0 is the susceptibility of the Heisenberg $S = {}^1/_2$ antiferromagnetic chain[23] and α is the fractional amount of paramagnetic impurities. Best agreement (solid curve in Figure 8) was found with $J/k = -56.6$ (3) K, $g = 2.336$ (6), and $\alpha = 0.013$, with use of data points above 30 K (the curve is calculated down to 12 K) from the sample with the smallest α value. No indication of three-dimensional order, due to interchain interaction, was seen in the susceptibility data above the lowest temperature measured (5 K).

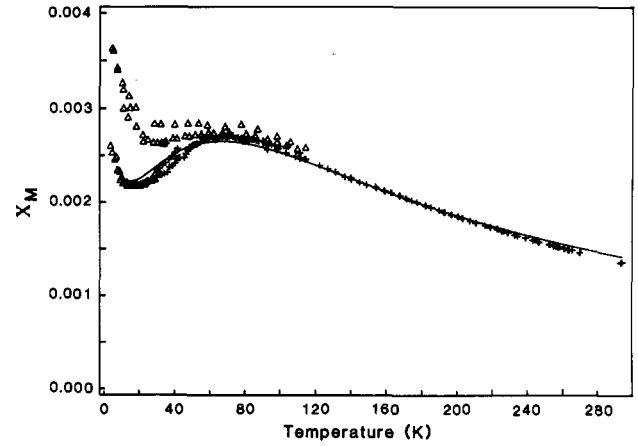

Figure 8. Molar powder susceptibility of 6MAPC. The low-temperature regime shows the results for several different samples. The solid curve was calculated as described in the text, with use of data points denoted by + symbols.

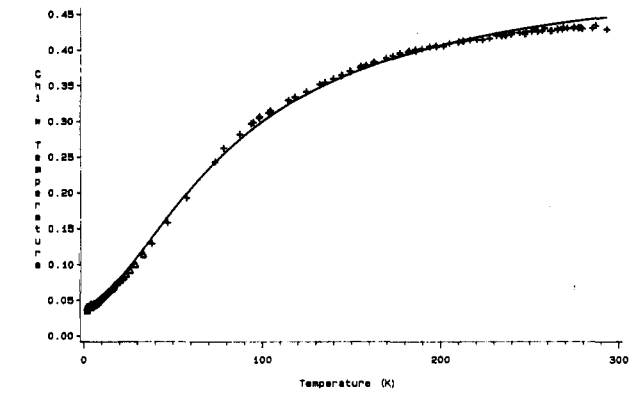

Figure 9. $\chi_m T$ vs. T for a powder sample of 4MAPC. The solid curve was calculated as described in the text, with use of data points denoted by + symbols.

The data for 4MAPC are shown in Figure 9. Without any doubt the effective moment, proportional to $(\chi T)^{1/2}$ is strongly reduced from Curie law, again indicating strong antiferromagnetic coupling. Using the one-dimensional Heisenberg model with a paramagnetic impurity as above,[23] best agreement is found with $J/k = -49.6$ (6) K, $g = 2.368$ (6), and $\alpha = 0.07$, when only data with $T > 15$ K are used.

For both compounds the g value does not exactly fit the high-temperature data. It seems that the reduction in the magnetic moment with lower temperature is too rapid for the Heisenberg model and that an artificially high g value (as compared to EPR data) compensates the wrong curvature. Comparison with figures in Bonner's review article[24] suggests that a slight amount of anisotropy in the exchange Hamiltonian would correct the mismatch, leading to a somewhat larger exchange constant and a smaller g value.

Magneto–Structural Correlation. One of the topics of current interest is the delineation of the relationships between structure and magnetic behavior in transition-metal salts.[3] The Cu(II) halide salts are particularly hard to characterize because of the wide variety of structural behavior exhibited. However, the series

(23) Bonner, J. C.; Fisher, M. E. *Phys. Rev.* [*Sect.*] *A* **1964**, *135*, A640.
(24) Bonner, J. C. *NATO ASI Ser., Ser. C* **1985**, *No. 140*, p 157 and references therein.

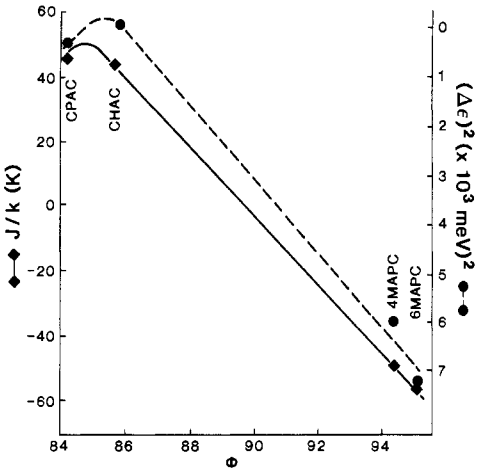

Figure 10. Plot of J/k (left-hand scale) and $(\Delta\epsilon)^2 \equiv (\epsilon_s - \epsilon_a)^2$ (right-hand scale) vs. bridging angle, ϕ, for CPAC, CHAC, 4MAPC, and 6MAPC.

of compounds presented in this paper (CPAC, CHAC, 4MAPC, and 6MAPC) are well-suited to the elucidation of a portion of these correlations because of the close relationship between the members. In each compound, the copper ion has a square-pyramidal geometry; the differences in the first coordination sphere, while crystallographically significant, are rather small (Table VIII). The major variation is the folding of the chain, defined by the angle δ between the normals to the basal planes of adjacent square pyramids. Since this is done without changing the coordination geometry substantially, the bridging Cu–Cl–Cu angles, ϕ, also change simultaneously.

The current basis for interpretation of magneto–structural correlation is the formulation of Hay, Thibeault, and Hoffmann,[25] who expressed the exchange coupling, J, in terms of the one-electron energies of the symmetric and antisymmetric MO's (ϵ_s and ϵ_a) found from the magnetic orbital on the individual metal ions. They obtained, for a dimer with one unpaired electron per metal ion

$$2J = 2K_{ab} - \frac{(\epsilon_s - \epsilon_a)^2}{J_{aa} - J_{ab}}$$

where K_{ab} is inherently positive and $J_{aa} - J_{ab} > 0$. Thus, the first term yields the ferromagnetic contribution to the exchange while the second term produces the antiferromagnetic contribution. It is assumed that K_{ab}, J_{aa}, and J_{ab} are relatively insensitive to small geometrical changes so that the variation in exchange is dictated primarily by the difference, $\Delta\epsilon$, between the two one-electron energies. It is noted that the antiferromagnetic contribution varies as $(\Delta\epsilon)^2$, so that a maximum ferromagnetic contribution is expected when $\epsilon_a = \epsilon_s$. Thus, for a given distortion path, a maximum in J may exist. An alternative formalism, emphasizing the role of overlap, has been given by Kahn.[26]

Calculations have been performed by Kahn et al.[27] using this latter approach for the folding of a copper dimer with a fixed square-planar coordination at the metal center. They indicated that interaction became more ferromagnetic as the dimer was folded. Bencini and Gatteschi[28] considered the folding of a dimer with square-pyramidal coordination but kept ϕ fixed as the dimer was folded. We have carried out an extended Hückel calculation[29] for dimer fragments with the actual geometry assumed by each of the four salts. As seen in Table VIII and Figure 10, good

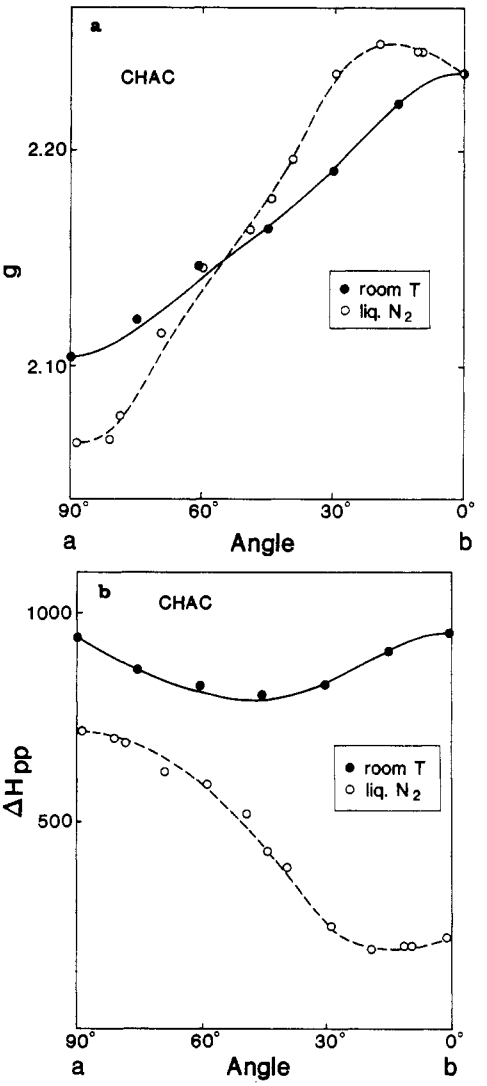

Figure 11. (a) EPR g value vs. crystal orientation in the ab plane for CHAC. (b) EPR line widths vs. crystal orientation in the ab plane for CHAC.

agreement with the experimental results are obtained. At large ϕ angles, $\epsilon_s - \epsilon_a$ is positive (ψ_a low in energy) and decreases as ϕ is decreased. $\Delta\epsilon$ changes sign at approximately 85° (~134°), at a geometry intermediate between those of CPAC and CHAC. Thus, the results indicate, for this section through the J hypersurface, the maximum value of J/k is approximately 50 K.

EPR Measurements

In this section of the paper, we report preliminary EPR studies on several of the compounds. The primary importance of these studies with respect to the thrust of this paper is information about the magnitude of the interchain coupling. This helps to define the degree of one-dimensionality of the systems. In addition, some comments concerning the temperature dependence of the EPR line widths, and their implications concerning the spin anisotropies, will be given. Two principal contributions to the line width data will be considered: spin anisotropy, which has a linear temperature dependence proportional to J^4, and the role of magnetically inequivalent subsystems.

CHAC. We begin by examining the EPR data for CHAC. Some results have been given by Poertadji et al.,[10] including the angular dependence of the g values and room-temperature line widths in the ac and bc planes, as well as the temperature dependence of the line widths for H_0 parallel to the a and c axes. However, they did not exploit the structural implication in their interpretation of the data, which obscured some of the more important conclusions. In addition, a rather thorough study of the low-temperature ($T \leq 4$ K) regime has been performed.[29]

(25) Hay, P. J.; Thibeault, S. C.; Hoffmann, R. *J. Am. Chem. Soc.* **1975**, *97*, 4884.
(26) Kahn, O. *NATO ASI Ser., Ser. C* **1985**, *No. 140*, 37.
(27) Charlot, M. F.; Kahn, O.; Jeannin, S.; Jeannin, Y. *Inorg. Chem.* **1980**, *19*, 1410.
(28) Bencini, A.; Gatteschi, D. *Inorg. Chim. Acta* **1978**, *31*, 11.
(29) Hoogerbeets, R. Ph.D. Thesis, University of Leiden, Leiden, The Netherlands, 1984.

In Figure 11, the angular dependence of EPR g values and line widths in the ab plane are presented, at both room temperature and 77 K. In that plane, two magnetically inequivalent chains are present. For each chain the projection of the axial Cu–Cl bond onto the ab plane makes alternating angles of +17 and −17° with the b axis. These two sets of chains are coupled by the weak antiferromagnetic coupling responsible for the metamagnetic behavior. If the coupling is less than the g anisotropy, two separate EPR lines will be anticipated. If it is greater, an averaged EPR line is anticipated.

At room temperature, the g value shows a monotonic increase as H_0 rotates from the a to the b axis, and the line widths are nearly independent of angle. However, the line widths are so large that it is impossible to distinguish between the two cases. It is noted that the g values do not show the normal $g^2(\theta) = (g_b^2 \cos^2 \theta + g_a^2 \sin^2 \theta)$ angular dependence. A much different picture emerges from the liquid-N_2 data. A maximum in g is observed near $\theta = 17°$ (measured from the b axis) and a minimum for the line width at the same angle. The line widths cover a large range (200–700 Oe) in the ab plane. The line shape is clearly distorted and appears to be a superposition of two (or more) lines. We have observed behavior like this previously.[30] In particular, when two lines of vastly different line widths overlap, the apparent line width as measured by the peak-to-peak separation in the first-derivative spectrum corresponds most nearly to that of the narrower line. On the other hand, the transition with the larger width manifests itself in the tail of the spectrum, leading to an apparently more Lorentzian line shape. Thus, it is concluded that two independent lines are observed and that $|J_{AF}| < (\Delta g/g)\hbar\omega$, or $|J_{AF}/k| < 0.05$ K. This is in agreement with the magnetic study ($J_{AF}/k \approx -0.05$ K). The ferromagnetic interchain coupling of ~0.5 K is between magnetically equivalent chains and thus will not influence line positions. In addition, since we expect a nearly uniaxial local environment at each copper site, with $g_\parallel > g_\perp$, the maximum g value of 2.248 corresponds to the $g_\parallel$ component (to be corrected, of course, for inclination of the tensor axis out of the ab plane). Thus, the narrow line width of ~200 Oe is associated with $g_\parallel$. The 77 K line widths in the bc plane (not shown), where the projection of the axial Cu–Cl bond now is tipped away from the b axis and all chains are magnetically equivalent, shows a similar effect.

Temperature Dependence of Line Widths in CHAC. In the temperature region between 77 and 300 K, the EPR line widths show a linear temperature dependence (Figure 12). This behavior is characteristic of copper halide salts with relative strong exchange coupling.[31] It has been attributed to the phonon modulation of the spin anisotropies.[32] In the presence of strong exchange coupling, the latter make the dominant contribution to the second moment, M_2, of the EPR line.[33] The magnitude of the spin anisotropy is generally assumed to be proportional to $|J|$. Thus, $M_2 \propto J^2$ so that the static EPR line width, ΔH, is given by

$$\Delta H_0 \approx M_2/|J| \propto |J|$$

The phonon modulation, however, yields a linear temperature dependence

$$\Delta H = \Delta H_0 + bT$$

where it has been shown that $b \propto J^4$. Thus, broad, temperature-dependent line widths are generally typical of strongly exchange coupled copper(II) salts.[34]

The spin anisotropies give rise to characteristic angular dependences of the EPR line widths. Defining the anisotropic exchange, D, and the antisymmetric exchange, $\vec{d}$, by the nearest-neighbor interaction spin Hamiltonian

$$\mathcal{H} = -2J\sum_{nn} S_i S_j + D\sum_{nn} S_i^z S_j^z + \sum_{nn} \vec{d}\cdot S_i \times S_j$$

where z denotes the direction of preferred spin orientation, it is found[33] that D and d_z give a maximum static line width and maximum temperature dependence along z while d_x and d_y give maximum contributions along the (magnetic) x and y directions.

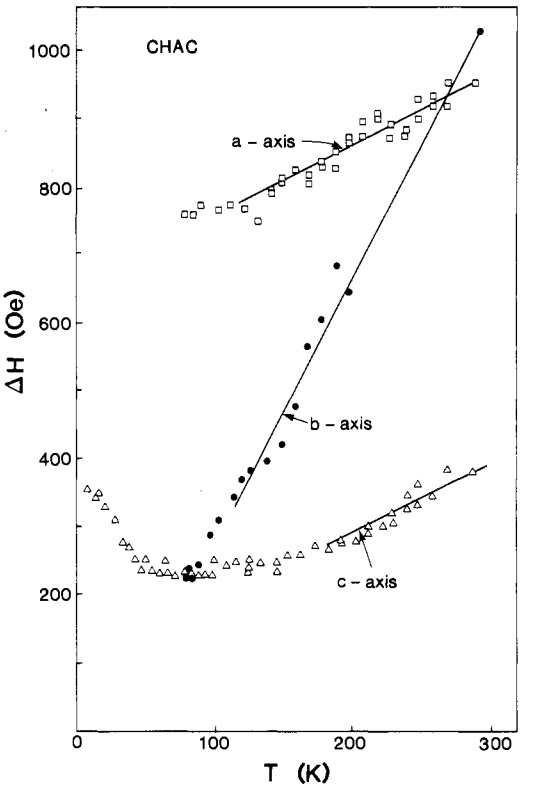

Figure 12. Temperature dependence of EPR line widths in CHAC along the a, b, and c crystallographic axes.

Experimentally, it is observed that the largest temperature dependence for CHAC occurs for the crystallographic b axis with smaller (~25%) effects along the a and c axes. CHAC is known to have a small (1–2%) Ising anisotropy with the b axis as the preferred spin direction,[8] as deduced from the bulk magnetic behavior. The spin canting behavior indicates that in the plane perpendicular to the chain (the ab plane) the local preferred direction is parallel to the projection of the axial Cu–Cl bond onto that plane. The projection of the axial Cu–Cl bond onto the ab plane makes an angle of about 15° with the b axis, in accord with the observed minimum in ESR line width at 15° (Figure 11). Neglecting this small difference between local and bulk axes in the following discussions, we conclude that the magnetic z axis is parallel to the crystallographic b direction. Thus, D and/or d_z make the maximum contribution to the line widths. The smaller temperature dependence along the a and c axes implies a smaller contribution from $\vec{d}$ in those directions. In fact, the component of $\vec{d}$ along the chain must be zero by symmetry, and since the temperature dependence along the a axis is only slightly larger than that along the c axis, we conclude that the x component of the antisymmetric exchange is small.

We note that the magnitude of the line widths along the a axis at liquid-nitrogen temperature is much larger than those along the other two directions. This is not consistent with having the sole contribution to the line widths arising from the spin anisotropies. The previous studies[10] have identified an unusual spin–lattice relaxation process in this system, and this may be the cause of abnormally large line widths parallel to the a axis.

6MAPC. The results of EPR measurements for the ac and bc planes of 6MAPC at room and liquid-nitrogen temperatures are shown in Figure 13. Some scatter in the apparent g values

(30) Willett, R. D.; Barberis, D.; Waldner, F. *J. Appl. Phys.* **1982**, *53*, 2677.
(31) Drumheller, J. E.; Dickey, D. H.; Reklis, R. E.; Zaspel, C. E.; Glass, S. J. *Phys. Rev. B: Solid State* **1972**, *5*, 4631.
(32) Willett, R. D.; Wong, R. J. *J. Magn. Reson.* **1981**, *42*, 446.
(33) Soos, Z. G.; McGregor, K. T.; Cheung, T. T. P.; Silverstein, A. J. *Phys. Rev. B: Solid State* **1977**, *16*, 3036.
(34) Another consequence is that this spin anisotropy contribution gives rise to large short-time correlations that obscure the long-time, diffusive behavior responsible for the characteristic line widths and line shapes in the low-dimensional system.

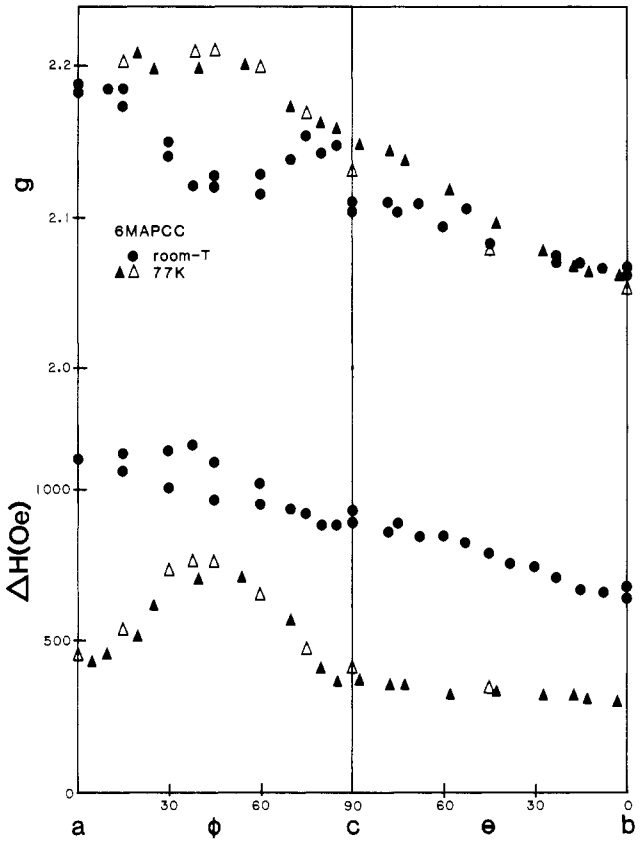

Figure 13. EPR g values (top) and line widths (bottom) vs. crystal orientation for 6MAPC in the *ac* and *bc* planes.

obtained at room temperature is noticeable. This is due to a combination of factors: the very broad lines, coupled with a ubiquitous narrower impurity ($CuCl_2 \cdot 2H_2O$) signal, made the definition of the center of the resonance unreliable. From the angular dependence of the values, however, we will deduce that the coupling between chains is less than 0.05 K.

The spectra yield $g_a = 2.19$, $g_b = 2.07$, and $g_c = 2.15$. Since the pseudo-C_4 axes are perpendicular to the b axis, we have $g_\perp = 2.07$. The $g_\parallel$ value can be estimated from g_a and g_c to be approximately 2.27. Within the *bc* plane, the chains are magnetically equivalent, and the g values show the normal angular dependence. In the *ac* plane, in contrast, the chains are not magnetically equivalent and anomalous behavior is seen, as with CHAC. At room temperature, the apparent g value reaches a minimum at $\phi \approx 50°$ while at 78 K it reaches a maximum at $\phi \approx 40°$. Recognizing that the pseudo-C_4 axes of the magnetically equivalent chains are oriented at $\phi \approx \pm 45°$, it is reasonable to assume that at room temperature the apparent center of the line reflects primarily the contribution from the chain with the $g_\perp$ signal whereas at 77 K the $g_\parallel$ transition of the other set of chains has sufficiently narrowed to dominate the apparent g value. Thus, it is again concluded in the EPR experiment that the chains behave independently so that $|J/k| \leq 0.05$ K.

As with CHAC, the major portion of the temperature dependence of the EPR line width can be accounted for by phonon modulation of the spin anisotropy, which leads to a linear temperature dependence of the line width.

Conclusions

The crystal structures of a new class of copper(II) halides have been presented. They are characterized by the existence of bibridged, uniform chains of copper(II) ions with square-pyramidal coordination geometry. Systematic variations in the coordination geometry are observed, with the $Cu-Cl_{eq}$ bond lengths and $Cl_{eq}-Cu-Cl_{ax}$ bond angles increasing as the $Cu-Cl_{ax}$ bond length shortens. The structures are stabilized by the existence of numerous $N-H\cdots Cl_{ax}$ hydrogen bonds so that it is not necessary for that chloride ion to participate in bridging to other copper(II) ions. In two of the salts (4MAPC and 6MAPC), the bridging Cu_2Cl_2 units are planar; in the other two salts (CHAC and CPAC), the bridging unit is folded across the Cl–Cl direction. This folding causes a substantial shortening of the Cu–Cu distance in the chain, as well as tipping of the $Cu-Cl_{ax}$ bond so that Cl_{ax} approaches the sixth coordination site on an adjacent copper(II) ion. Continued folding would lead to the formation of a tribridged chain, as seen in a number of other salts. The interrelations between these new types of chains, the tribridged chain, and the bibridged dimer chains were explored, pointing out the competitive nature of hydrogen-bonding interactions vs. bridging in determining the type of chain assumed.

These compounds have provided a system to probe magneto–structural correlations in a systematic manner. Experimentally it is observed that the exchange coupling in the chain is ferromagnetic for bridging angles near 85° and antiferromagnetic for angles near 95°. Comparison with theory supports the fact that the antiferromagnetic contribution is near zero for CHAC and CPAC. Assuming that the ferromagnetic contribution to that exchange, as expressed in the Hoffmann formalism, is nearly independent of geometry, it may be anticipated that the maximum value of the ferromagnetic coupling constant, J/k, in copper(II) chloride salts will be approximately 50 K. With the exception of $3CuCl_2 \cdot 2diox$[35] (diox = 1,4-dioxane), this appears to be true.[3]

Both CHAC and CPAC exhibit metamagnetic behavior in the low-temperature ordered magnetic phase. Thus, the coupling between chains via the hydrogen-bonding network is ferromagnetic. The existence of ferromagnetic behavior for a complex exchange pathway involving Cu–Cl–H–N–H–Cl–Cu interactions is quite surprising, although not without precedent. In $[(CH_3)_3NH]MCl_3 \cdot 2H_2O$ salts, a M–O–H–Cl–H–O–M pathway leads to ferromagnetic interchain coupling.[36] In the case of CHAC and CPAC, the crucial factor is undoubtedly that the axial chloride ions are involved in the exchange pathway. Thus, the pathway is orthogonal to the magnetic orbitals on the two copper ions involved.

The compounds 4MAPC and 6MAPC are shown to be excellent one-dimensional antiferromagnets. Although the three-dimensional ordering was not detected, the upper limit on J' deduced from the EPR studies ($|J'/k| < 0.05$ K) indicates that $|J'/J| < 10^{-3}$. While better spin $^1/_2$ Heisenberg antiferromagnetic 1D systems are known, the *n*MAPC salts can be grown as large single crystals, a distinct advantage for various types of neutron-scattering investigations.

The results presented in this paper confirm the utility of using large, bulky organic cations to synthesize low-dimensional magnetic systems. As more of these types of systems are prepared and studied, it will be possible to obtain a more detailed understanding of the factors that affect magneto–structural correlation in them. These types of compounds should be extremely useful for the solid-state physics community as realizations of theoretical models that have predicted unusual critical point, phase transition, and excitation (solitons) behavior.

Acknowledgment. This work was supported by NSF Grant DMR 8219430. The Nicolet R3m/E facility was established through funds provided by NSF Grant CHE 8408407 and by Boeing Co.

Registry No. CPAC, 104439-70-5; 6MAPC, 89820-69-9; 4MAPC, 89820-68-8; CHAC, 74018-74-9.

Supplementary Material Available: Listings of anisotropic thermal parameters and H atom coordinates and isotropic thermal parameters (2 pages); listings of observed and calculated structure factors (18 pages). Ordering information is given on any current masthead page.

(35) Livermore, J. C.; Willett, R. D.; Gaura, R. M.; Landee, C. P. *Inorg. Chem.* **1982**, *21*, 1403.
(36) For a review see: Willett, R. D.; Gaura, R. M.; Landee, C. P. In *Extended Linear Chain Compounds*; Miller, J. S., Ed.; Plenum: New York, 1983; Vol. 3, p 143.